Cell Reports

Allele-Specific DNA Methylation and Its Interplay with Repressive Histone Marks at Promoter-Mutant *TERT* Genes

Graphical Abstract

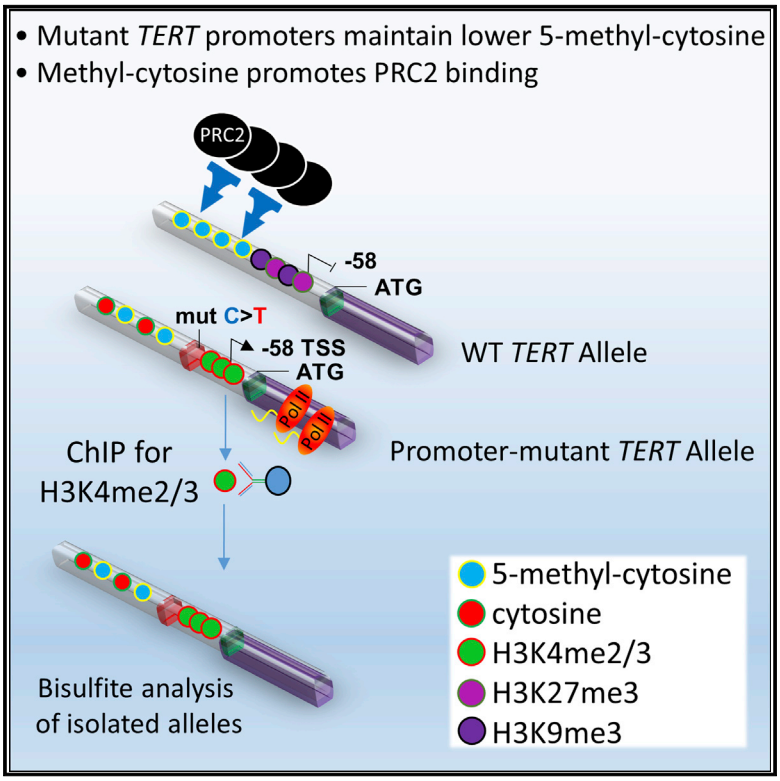

Highlights

- Promoter mutant *TERT* genes show allele-specific DNA hypomethylation
- This is opposite to the situation in cancers without *TERT* promoter mutations
- Methyl-CpG enhances PRC2 binding, suggesting causal link to histone methylation
- *TERT* CpG island methylation correlates with patient survival in several cancers

Authors

Josh Lewis Stern, Richard D. Paucek, Franklin W. Huang, Mahmoud Ghandi, Ronald Nwumeh, James C. Costello, Thomas R. Cech

Correspondence

thomas.cech@colorado.edu

In Brief

The promoter for a telomerase gene (*TERT*) is the third most frequently mutated site in cancer. These mutations drive unusual expression of TERT from a single allele, allowing unceasing cell division. Stern et al. identify modifications of the promoter that appear to collaborate to maintain this expression pattern in these cancers.

Stern et al., 2017, Cell Reports *21*, 3700–3707
December 26, 2017
https://doi.org/10.1016/j.celrep.2017.12.001

CellPress

OPEN ACCESS
CellPress

Cell Reports
Report

Allele-Specific DNA Methylation and Its Interplay with Repressive Histone Marks at Promoter-Mutant *TERT* Genes

Josh Lewis Stern,[1] Richard D. Paucek,[1] Franklin W. Huang,[2,3] Mahmoud Ghandi,[2] Ronald Nwumeh,[1] James C. Costello,[4] and Thomas R. Cech[1,5,*]

[1]BioFrontiers Institute, Department of Chemistry and Biochemistry, and Howard Hughes Medical Institute, University of Colorado Boulder, Boulder, CO 80303, USA
[2]Broad Institute of Harvard and MIT, Cambridge, MA 02142, USA
[3]Department of Medical Oncology, Dana-Farber Cancer Institute, Boston, MA 02115, USA
[4]Department of Pharmacology and University of Colorado Comprehensive Cancer Center, University of Colorado, Anschutz Medical Campus, Aurora, CO 80045, USA
[5]Lead Contact
*Correspondence: thomas.cech@colorado.edu
https://doi.org/10.1016/j.celrep.2017.12.001

SUMMARY

A mutation in the promoter of the Telomerase Reverse Transcriptase *(TERT)* gene is the most frequent noncoding mutation in cancer. The mutation drives unusual monoallelic expression of *TERT*, allowing immortalization. Here, we find that DNA methylation of the *TERT* CpG island (CGI) is also allele-specific in multiple cancers. The expressed allele is hypomethylated, which is opposite to cancers without *TERT* promoter mutations. The continued presence of Polycomb repressive complex 2 (PRC2) on the inactive allele suggests that histone marks of repressed chromatin may be causally linked to high DNA methylation. Consistent with this hypothesis, *TERT* promoter DNA containing 5-methyl-CpG has much increased affinity for PRC2 *in vitro*. Thus, CpG methylation and histone marks appear to collaborate to maintain the two *TERT* alleles in different epigenetic states in *TERT* promoter mutant cancers. Finally, in several cancers, DNA methylation levels at the *TERT* CGI correlate with altered patient survival.

INTRODUCTION

TERT encodes the catalytic subunit of telomerase, the ribonucleoprotein complex that maintains telomere length in stem cells and most cancer cells (Counter et al., 1992). Multiple cancers show unusual monoallelic activation of *TERT* by the *de novo* acquisition of a C > T transition on one *TERT* promoter (Horn et al., 2013; Huang et al., 2013, 2015; Killela et al., 2013; Stern et al., 2015). These mutations occur at −124 (occasionally at −146) bp from the translational start site and provide a new binding site for the GABPA/B1 transcription factor; the transcriptionally inactive *TERT* promoter in the same cell bears the H3K27me3 repressive mark (Bell et al., 2015; Stern et al., 2015). In many other cancers, TERT is expressed biallelically or monoallelically by molecular mechanisms that remain poorly understood (Huang et al., 2015).

In addition to H3K27me3, 5-methyl-cytosine (5mC) at CpG dinucleotides is a canonical epigenetic mark of transcriptional silencing (Baylin et al., 1998; Herman, 1999; Herman et al., 1998; Laird and Jaenisch, 1996; Merlo et al., 1995). Here, however, the *TERT* gene has been an outlier. *TERT* expression in most previously studied cancers is associated with increased 5mC in the *TERT* promoter CpG island (CGI) (Barthel et al., 2017; Dessain et al., 2000; Devereux et al., 1999) Thus, in these cancers, *TERT* transcription occurs despite this gain of 5mC. To explore this non-canonical relationship with 5mC in more detail, we chose to study cancers with heterozygous −124 mutations, capitalizing on the fact that these cells contain *TERT* alleles maintained in different transcriptional states. We reasoned that, if *TERT* CGI methylation were a positive regulator of TERT mRNA expression in these cells as suggested by previous studies (e.g., Barthel et al., 2017), we should observe higher levels of 5mC on the active promoter mutant allele.

Contrary to this expectation, our results indicate that 5mC levels at the *TERT* promoter in cancers with heterozygous −124 mutations are maintained at lower levels on the active allele than on the transcriptionally silent allele. This finding is consistent with the canonical influence of 5mC on transcription. Thus, *TERT* promoters with −124 mutations exhibit divergent regulatory dynamics compared to those with wild-type (WT) promoters. We find that the EZH2 subunit of PRC2, the enzyme responsible for deposition of H3K27me3, resides at the inactive *TERT* allele. Testing for a causal relationship between DNA methylation and histone methylation, we show that PRC2 displays a strong binding preference for methylated *TERT* promoter DNA *in vitro*. This suggests a regulatory circuit, wherein low 5mC discourages PRC2 binding on active *TERT* alleles in these −124 cancers.

RESULTS

Distinct 5mC Levels at the *TERT* CGI in −124 Cancers

The *TERT* promoter contains a CGI that is methylated in cancer, and the entire feature extends from near chromosome (chr)

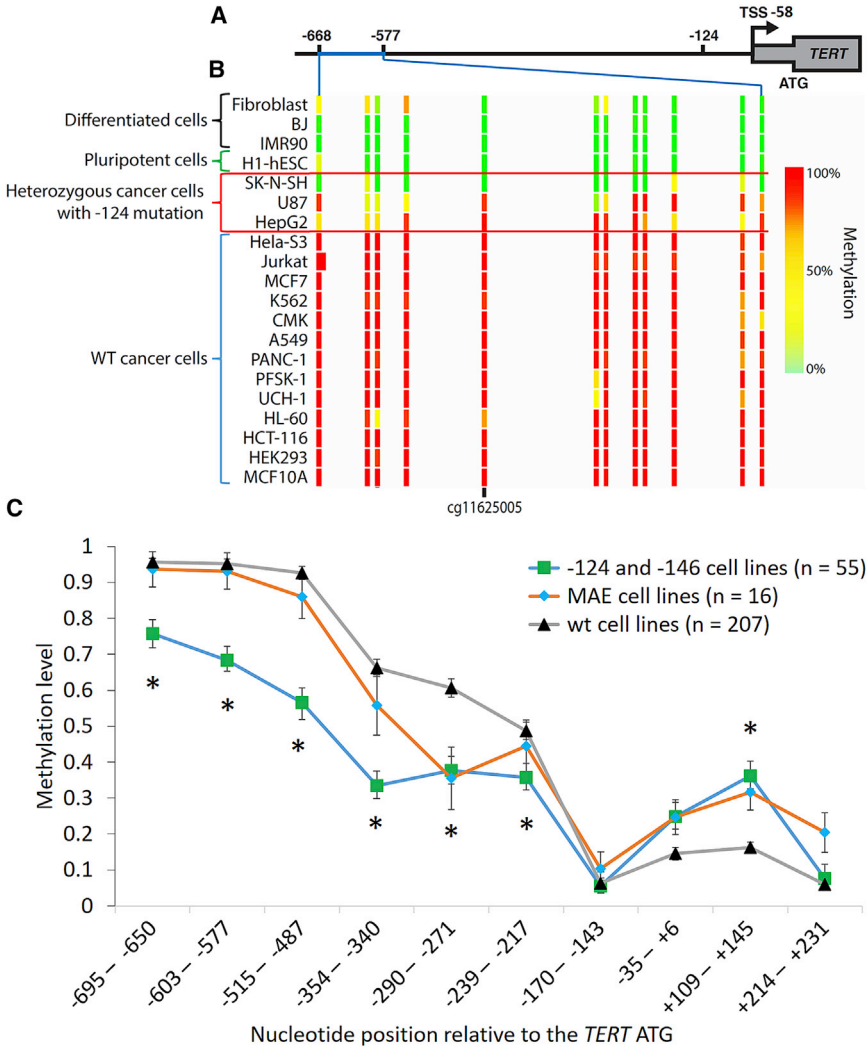

Figure 1. 5mC Levels at the *TERT* Promoter CGI Are Reduced in Cell Lines with −124 Mutations

(A) The position of the *TERT* CGI relative to the −124 mutation, transcription start site (TSS), and ATG. The region of the *TERT* CGI displayed extends from −668 to −577 (chr5:1,295,681-1,295,772 in HG19).

(B) ENCODE RRBS data indicate reduced 5mC at the CGI in −124 heterozygous cells versus cancer cells with WT promoters. The position of cg11625005 is indicated (−633 from the *TERT* ATG).

(C) Relative DNA methylation levels across the *TERT* CGI in CCLE cell lines (n = 278). Cell lines are grouped by *TERT* promoter mutation status and monoallelic *TERT* expression status (MAE, WT promoter with monoallelic expression). Each value derives from RRBS data from one CpG or more; CpGs were pooled was based on nucleotide proximity. Data indicate median ± SEM. Significance test (see Experimental Procedures) compared WT and −124/−146 cell lines. *p < 0.05. hESC, human embryonic stem cell.

See also Figure S1 and Table S1.

5:1296000 (−838 relative to the *TERT* ATG) to a position near the end of exon 2 (chr5:1293450). We first studied 5mC levels in the promoter region of the *TERT* CGI using ENCODE reduced representation bisulfite sequencing (RRBS) data generated on a wide variety of primary cells and tumor-derived cell lines (Figures 1A and 1B; Table S1A). We observed a nearly uniform lack of methylation in this region of the *TERT* CGI in primary cells (e.g., fibroblasts, BJ cells, IMR90) (Figure 1B). In contrast, a nearly uniform gain of 5mC characterized the tumor-derived lines.

Upon closer examination, it appeared that the three cell lines with −124 mutations (HepG2, U87 MG, and SK-N-SH) exhibited intermediate or low levels of methylation at cg11625005 (Figure 1B). We then examined unpublished RRBS data for 55 tumor-derived cell lines with −124 or −146 mutations in the Cancer Cell Line Encyclopedia (CCLE) and compared them with 207 cell lines lacking *TERT* promoter mutations (Figures 1C and S1). These cell lines were derived from a very broad range of cancer types (Table S1B). The data indicate that the average level of 5mC is significantly lower in the lines with mutated *TERT* promoters starting from around −220 bp upstream of the *TERT* ATG through −700 bp and significantly higher within exon 1 (+109 to +145; Figure 1C; Table S2).

Some cancer cell lines show monoallelic expression (MAE) of *TERT* even in the absence of promoter mutations (Huang et al., 2015). This phenotype suggested that the epigenetic conditions that facilitate *TERT* expression in these cells might be distinct from those with WT promoters that express *TERT* biallelically or cancers with promoter mutations. Therefore, we examined DNA methylation in 16 cell lines with MAE and found methylation levels resembling the WT cell lines at many nucleotide positions (Figures 1C and S1). At two positions (−290 to −271 and +109 to +145), however, the MAE cells converged with the epigenotype of *TERT* promoter mutants, suggesting that these positions may be important for monoallelic expression.

To assess whether patient tumor samples in The Cancer Genome Atlas (TCGA) recapitulated the observed reduction in methylation in the *TERT* CGI seen in these promoter mutant cell lines, we combined −124 genomic profiling with *TERT* promoter 5mC from the Illumina Infinium HumanMethylation450 BeadChip array at cg11625005 (a specific CpG dinucleotide at −634). We compared patient tumor samples with −124 mutations to samples without mutations in cutaneous melanoma, liver cancer, and bladder cancer. Despite the Infinium array data comprising both active and inactive alleles, we detected significantly reduced levels of methylation at cg11625005 in −124 tumors (Figure S2). Thyroid cancer and lower grade glioma did not display the same relationship between 5mC and

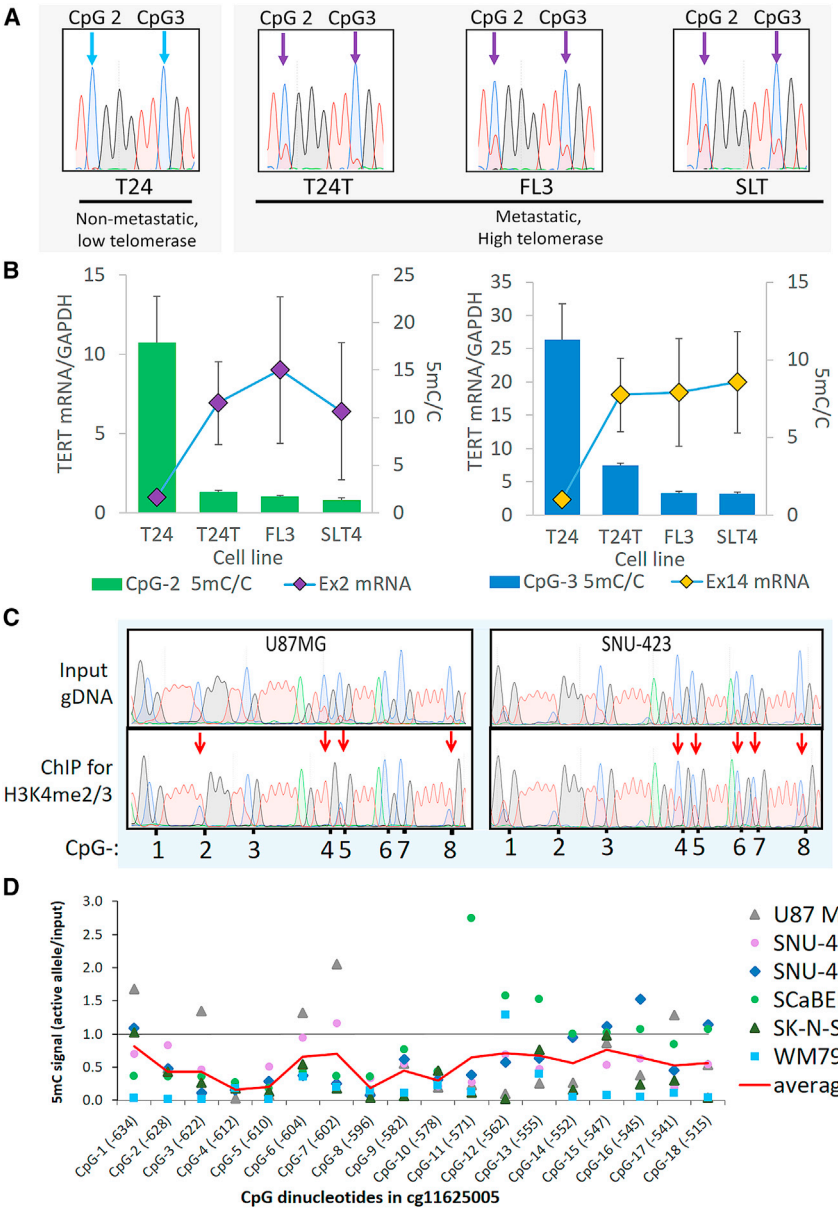

Figure 2. Hypomethylation of the *TERT* CGI at −450 to −750 Is Specific to Active Alleles and Associates with Higher TERT mRNA in a Panel of Related −124 Mutant Bladder Cancer Cell Lines

(A) Sanger sequencing traces of bisulfite-converted genomic DNA from the low-telomerase, non-metastatic −124 heterozygous bladder cancer line T24 versus its metastatic, high-telomerase relatives (FL3, SLT4, and T24T). After bisulfite conversion, the ratio of the blue peak (C) to the red peak (T) at CpG sites indicates the 5mC/C ratio (see Figure S3B). Thus, T24 cells are mostly methylated at CpG-2 and CpG-3 (blue arrows), and the other lines are partially hypomethylated (purple arrows). CpG numbers refer to positions in (D).

(B) T24 lines display an inverse relationship between 5mC at CpG-2 and CpG-3 within the *TERT* CGI versus TERT mRNA expression measured at exon 2 (Ex2) and exon 14 (Ex14). Additional CpGs displayed a similar pattern (Figure S3A). 5mC data indicate mean + SEM (n = 4), and TERT expression data indicate mean ± SEM (n = 3–7).

(C) Representative Sanger sequencing traces of bisulfite-converted DNA from input genomic DNA or H3K4me2/3 ChIP-isolated DNA from two cell lines quantified in (D). Red arrows indicate reduced 5mC in ChIP DNA. Numbers below traces give relative positions of the CpG in the *TERT* CGI, as annotated in (D). gDNA, genomic DNA.

(D) Mean 5mC levels in H3K4me2/3 ChIP-isolated DNA versus input DNA (see Figures S3C and S3D for individual cell lines and measures of variance). Each cell line bears heterozygous mutations at −124. A ratio of 1 indicates no difference in 5mC levels between input and ChIP DNA. Methylation on the actively transcribed allele across all cell lines was significantly lower (one-sample t test, $p < 0.001$) compared to the expected value of 1. One CpG dinucleotide in particular (CpG-4) was consistently under-methylated ($p < 0.0001$). The six heterozygous lines analyzed were U87 MG (glioblastoma), SK-N-SH (neuroblastoma), the HCC lines SNU-475 and SNU-423, melanoma (WM793), and the bladder carcinoma line SCaBER. CpG-1 is cg11625005. The red line indicates the average for the six lines.

See also Figure S3.

the −124 mutation, although both of these tumor types exhibited conspicuously low TERT mRNA, and thyroid cancer also displayed overall anomalously low levels of DNA methylation (Figure S2B).

Higher *TERT* Transcription in Bladder Cancer Cell Lines Associates with Reduced 5mC in the *TERT* CGI

The aforementioned data indicate that both −124 mutant tumors and −124 cell lines exhibit distinct methylation patterns at the *TERT* CGI, compared to tumors and cell lines with WT promoters. Given the importance of promoter DNA methylation in regulating transcription, we measured *TERT* CGI methylation and transcription in a panel of related −124 mutant bladder cancer cell lines. T24 bladder carcinoma cells are a non-metastatic-tumor-derived cell line; T24T is a metastatic relative of T24 and was subsequently passaged in mice to obtain the metastatic lines FL3 and SLT4 (Gildea et al., 2000, 2002). Bisulfite sequencing analysis indicated that T24 exhibited the highest level of 5mC at the *TERT* CGI, while the other three lines exhibited decreased levels of 5mC at specific CpG dinucleotides (Figures 2A and S3A). T24 expresses low levels of the telomerase enzyme, while FL3, SLT4, and T24T express much higher levels (Borah et al., 2015). We assessed the level of TERT mRNA in these cells and found that the levels were highest in the metastatic derivative lines (Figure 2B). Thus, levels of 5mC at this locus are negatively correlated with TERT mRNA expression in this series of related bladder cancer lines.

Reduced 5mC Characterizes the −124 Mutant *TERT* Alleles

Because the levels of 5mC described in the previous datasets are a composite of both transcriptionally active and inactive alleles, we considered the possibility that tumor-derived −124 cells may have allele-specific reduction of methylation. To isolate the active alleles for bisulfite sequencing analysis, we used chromatin immunoprecipitation (ChIP) using anti-H3K4me2/3 antibodies (Stern et al., 2015) in six −124 cell lines. DNA fragments isolated by ChIP were subjected to bisulfite sequencing. Bisulfite conversion results in the transition of cytosine to thymine only in the absence of 5mC; methylated cytosines are protected from this chemical reaction. Therefore, for each nucleotide position, the level of 5mC in ChIP samples relative to input samples can be assessed by quantifying the peak height of unconverted cytosine relative to thymine. For each sequencing sample, the bisulfite conversion was efficient, as assessed by the complete conversion of neighboring non-CpG cytosines. Quantification of these data across the six cell lines revealed that the H3K4me2/3-associated active alleles commonly exhibited lower levels of CpG methylation at many positions in the *TERT* CGI (Figures 2C, 2D, and S3C). Note that these results are opposite to the expectation from the literature of increased *TERT* gene expression correlating with high CpG methylation in other cell types (Barthel et al., 2017; Guilleret and Benhattar, 2004), but they are consistent with our data on the four related bladder cancer lines (Figures 2A and 2B). To provide additional confidence in this conclusion, we cloned the PCR products from four cell lines from input and H3K4me2/3 ChIP products (Figure S3D). The observation of higher methylation in the input samples than in the ChIP samples supports our conclusion that reduced methylation characterizes the transcribed alleles in these heterozygous cell lines.

EZH2 Is Preferentially Associated with the Silent *TERT* Allele

Previously, we have described that transcriptionally inactive alleles in cancers with −124 mutations bear the H3K27me3 histone mark (Stern et al., 2015), which is one of the two canonical histone marks of repressive chromatin. The enzyme responsible for the deposition of H3K27me3, enhancer of zeste homolog 2 (EZH2), is the catalytic subunit of the PRC2 complex. To test whether EZH2 exhibited allele-specific recruitment at *TERT*, we performed ChIP using antibodies directed against histone marks or EZH2, followed by DNA purification, PCR, and Sanger sequencing. While DNA purified from chromatin prior to ChIP displayed both alleles in sequencing traces, ChIP for both H3K27me3 and EZH2 exhibited enrichment for the CCCTCC sequence (Figures 3A and 3B) diagnostic of the silent allele. Thus, in these cells at this locus, PRC2 exhibits a preference for occupying the inactive *TERT* allele. The second major histone mark of repressive chromatin, tri-methylated H3K9, can co-occur with H3K27me3 (Mozzetta et al., 2015). Allele-specific ChIP using antibodies against H3K9me3 showed that it was also enriched on the inactive WT *TERT* promoter in these cells (Figure 3B). Therefore, the inactive *TERT* promoter is the target of both PRC2 and the enzymes responsible for deposition of H3K9me3, such as G9a, SetDB1, and SUV39H1 and -H2 (Greer and Shi, 2012).

Because cell lines with WT *TERT* promoters typically exhibit much higher levels of 5mC at the promoter (Figure 1B), we tested whether this might correlate with relatively higher levels of EZH2 recruitment. Therefore, we performed EZH2 ChIP in three lines with WT promoters: HeLa, SNU-449, and HEK293T. In addition, since the heterozygous liver cancer cell line HepG2 displays relatively higher levels of 5mC for a *TERT* promoter mutant line, we also tested EZH2 occupancy in this line. Each of these lines displayed relatively high levels of EZH2 at the *TERT* promoter (Figure S4B), compared to the heterozygous lines (Figure 3C). To further test the relationship between EZH2 and 5mC, we analyzed ENCODE ChIP-seq data for HepG2, for which 5mC data are also available (Figure S4C). These data indicate that both 5mC and EZH2 levels are higher in the 5′ region of the *TERT* CGI, while levels of both are reduced near the *TERT* transcription start site (TSS). Because the active allele in HepG2 cells is likely to contribute relatively little signal to these ChIP-seq data, and as we have demonstrated that in heterozygous lines the active allele is hypomethylated, we conclude that the levels of 5mC and EZH2 are correlated at this locus in this liver cancer cell line.

5mC Enhances PRC2 Binding to *TERT* Promoter DNA *In Vitro*

Given that the inactive *TERT* allele in the −124 mutant cells accumulates both 5mC and H3K27me3, as well as EZH2, we hypothesized that a functional relationship may exist between these marks of inactive chromatin. Indeed, a number of studies have addressed the relationship between DNA methylation and repressive histone marks (Bartke et al., 2010; Lynch et al., 2012). Therefore, we tested whether 5mC modification of DNA affects PRC2 binding *in vitro*. We purified a recombinant human five-protein PRC2 complex (EZH2, SUZ12, EED, RBBP4, and AEBP2; Figure S4A) and used electrophoretic mobility shift assays (EMSAs) to test its ability to bind to either a fully unmethylated or a fully methylated *TERT* CGI DNA. PRC2 displayed >30-fold higher affinity to the 5mC-modified region of the *TERT* promoter over the unmethylated DNA (Figures 3D and 3E). These data suggest a positive feedback relationship whereby reduced 5mC methylation at an active *TERT* locus may discourage PRC2 recruitment.

5mC Levels at the *TERT* CGI Associate with Patient Survival in Multiple Cancers

Methylation levels at cg11625005 are negatively correlated with patient survival in some cancers (Castelo-Branco et al., 2013, 2016; Gojo et al., 2017). Therefore, we analyzed overall survival (OS) with respect to methylation and *TERT* promoter mutation in patient samples for a range of cancers within the TCGA. We first analyzed the data for cutaneous melanoma (SKCM) and found that samples with cg11625005 methylation beta values $\geq$ 0.75 showed a trend toward poorer survival, with borderline statistical significance ($p = 0.058$) (Figure 4). Therefore, we analyzed the remaining cancer types using this threshold. These analyses revealed that, in hepatocellular carcinoma (HCC) (liver hepatocellular carcinoma [LIHC], in which −124 mutations are common) and kidney renal papillary cell carcinoma (KIRP, in which −124 mutations are uncommon),

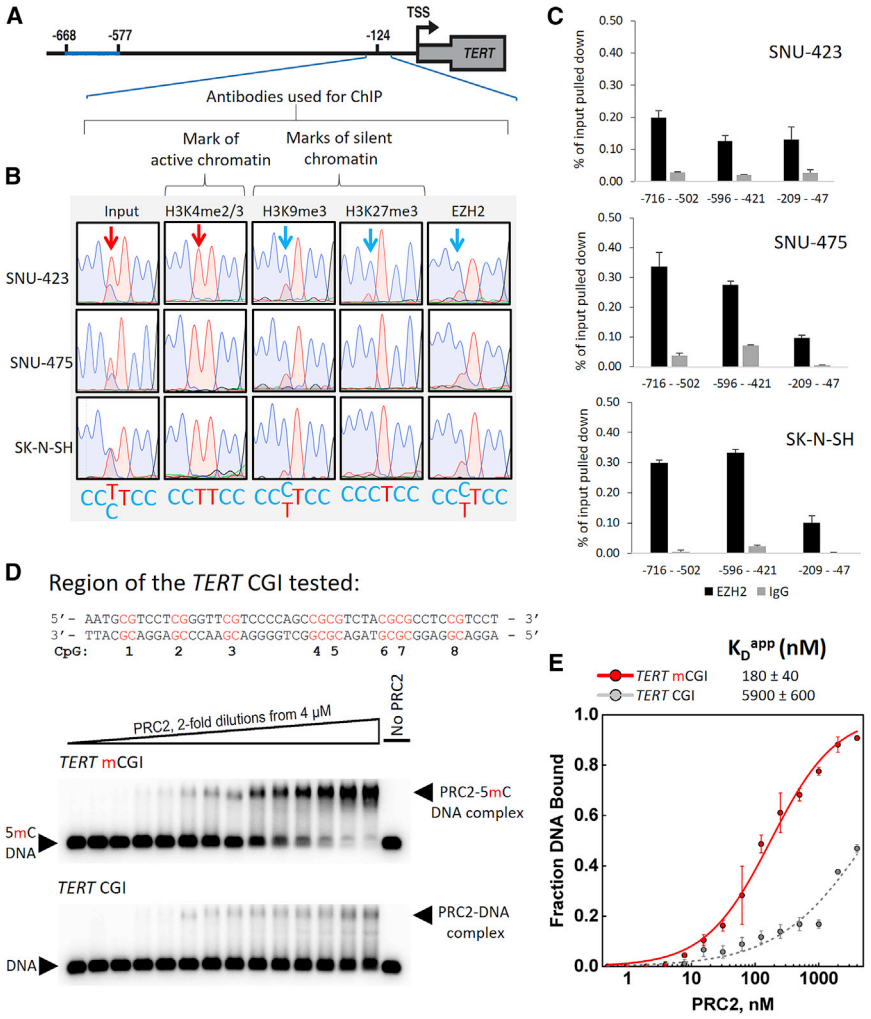

Figure 3. PRC2 Displays a Strong Binding Preference for 5mC-Rich *TERT* Alleles *In Vivo* in −124 Cells and Methylated *TERT* CGI DNA *In Vitro*

(A) Schematic illustrating the position of the allele-specific ChIP analysis (−209 to −47).

(B) Representative Sanger sequencing traces from DNA isolated by ChIP and amplified by three PCR reactions pooled prior to sequencing, showing the presence of H3K27me3, H3K9me3, and EZH2 on the inactive allele in HCC (SNU-423 and SNU-475) and neuroblastoma (SK-N-SH) −124 heterozygous tumor-derived cell lines. Arrows indicate the position of the heterozygous −124 mutation.

(C) Quantitative assessment of EZH2 occupancy of *TERT* promoters in three −124 mutant cell lines. Data indicate mean + SEM; n = 3 technical replicates. IgG, immunoglobulin G.

(D) Sequence tested for PRC2 binding *in vitro*. CpG numbers correspond to those listed in Figure 2D. Representative EMSA gels show binding of purified recombinant human PRC2 to the fully CpG-methylated *TERT* DNA versus the same sequence lacking 5mC modifications.

(E) Binding data fit with equilibrium binding curves. Error bars indicate ±SD (n = 3 independent experiments). K_D^{app}, K_D apparent.

patients with methylation above 0.75 at cg11625005 had significantly poorer overall survival. In contrast, patients with stomach adenocarcinoma (STAD; in which −124 mutations are uncommon) exhibited significantly better survival (Figure 4). STAD not only exhibited an opposite relationship between 5mC and survival compared to LIHC and KIRP, but also had an opposite relationship between EZH2 expression levels and overall survival (Figure S4D). These data suggest that the processes underlying *TERT* CGI hypermethylation and genome-wide activity of PRC2 may be linked and are indicative of altered patient survival in these cancers.

DISCUSSION

A key question in understanding the indefinite proliferation of cancer cells is how they regulate the expression of their telomere maintenance machinery. Most cancers activate *TERT* expression, either biallelically through poorly understood mechanisms or monoallelically, driven in many cases by heterozygous promoter mutations. Here, we find that a major arm of epigenetic gene regulation, CpG methylation, exhibits opposing dynamics in cancers with heterozygous −124 mutations compared to cancers with WT *TERT* promoters. Thus, the machinery maintaining the immortal phenotype in these two classes of cancers is distinct. Reduced 5mC in the *TERT* promoter has been reported previously for isolated subtypes of cancers with −124 mutations (Fan et al., 2016; Lindsey et al., 2014), although the allele specificity of 5mC has not previously been reported. Our analyses of large datasets of clinical samples broaden these findings to numerous cancers across many tissue types and provide a mechanistic rationale for how DNA methylation may affect *TERT* gene silencing in −124 cancers.

Cancers with heterozygous −124 mutations also exhibit allele-specific deposition of H3K27me3 by EZH2/PRC2, as well as deposition of H3K9me3 (Figure 3B). Intriguingly, there is a direct mechanistic relationship between H3K9me3 and the enzymatic machinery responsible for the 5mC modification (Cedar and Bergman, 2009; Epsztejn-Litman et al., 2008; Liu et al., 2013; McGarvey et al., 2006; Rose and Klose, 2014; Rothbart et al., 2012, 2013; Schübeler, 2015; Smith and Meissner, 2013) suggesting that the presence of H3K9me3 on the inactive allele could promote the accumulation of 5mC at the *TERT* promoter.

Repression facilitated by EZH2/PRC2 at the *TERT* locus may also be directly linked to CpG methylation (Figure 3), with the specificity for 5mC possibly conferred by the AEBP2 subunit of PRC2 (Wang et al., 2017). Preferential PRC2 binding to methylated *TERT* CGI DNA is likely to be

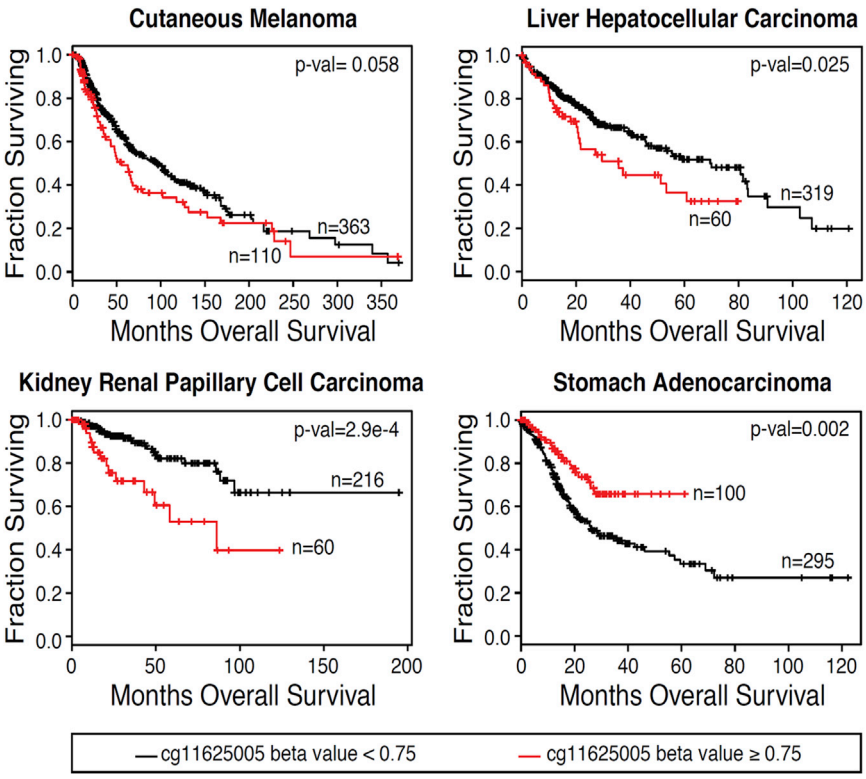

Figure 4. High Levels of 5mC at cg11625005 Correlate with Differences in Patient Survival in Specific Cancers

Kaplan-Meier plots were generated for TCGA patient data with cancers that commonly harbor *TERT* promoter mutations (HCC, LIHC, and cutaneous melanoma [SKCM]) and cancers that do not typically harbor *TERT* promoter mutations (kidney renal papillary cell carcinoma, KIRP; stomach adenocarcinoma, STAD). Patients were stratified based on methylation (beta value) at cg11625005. Statistical comparison was done using the log-rank test (see Experimental Procedures for details).

locus dependent, because, in other cases, PRC2 has been found to bind unmethylated CpG-rich chromatin (Bartke et al., 2010; Lynch et al., 2012). Factors other than CpG methylation certainly affect the level of PRC2 occupancy at any given locus *in vivo*.

Our data reveal that cell lines with MAE expression exhibit 5mC levels similar to that of WT *TERT* promoters at many CpG positions, but at specific loci (−290 to −271 and +109 to +145), they closely resemble *TERT* promoter mutants. The higher level of methylation within exon 1 (+109 to +145) for cells expressing TERT monoallelically (with or without promoter mutations) may represent a mechanism to increase the fidelity of transcription initiation (Maunakea et al., 2010; Neri et al., 2017), perhaps to more efficiently utilize their single active *TERT* allele.

The association between 5mC levels at the *TERT* promoter and either poorer overall survival in liver cancer and kidney renal papillary cell carcinoma or significantly improved overall survival in patients with stomach adenocarcinoma, suggests that these epigenotypes may be relevant to cancer progression. Association between higher methylation at cg11625005 and poorer patient survival has been previously reported (Castelo-Branco et al., 2013, 2016; Gojo et al., 2017; Seynnaeve et al., 2017); our results extend these findings to two additional cancer types, suggesting that hypermethylation of the *TERT* promoter may represent a broadly applicable prognostic marker. Our data show a more positive outcome for stomach adenocarcinoma patients with higher methylation at cg11625005 or with high EZH2 expression and suggest that the mechanisms driving survival in these patients may be distinct.

In conclusion, we find that *TERT* promoters in cancers with −124 mutations exhibit allele-specific chromatin and DNA modifications that differ from those on active *TERT* genes in cancers with WT promoters. These findings implicate multiple mechanisms by which cancers reactivate or maintain TERT expression to achieve telomere maintenance and immortalization. Such information may be clinically relevant, because inhibitors for both 5mC deposition and EZH2 are being developed for cancer therapy (Pfister and Ashworth, 2017).

EXPERIMENTAL PROCEDURES

Further details and an outline of resources used in this work can be found in the Supplemental Experimental Procedures.

Statistical Methods

For CCLE samples, comparisons were made using the Wilcoxon rank-sum test. The cg11625005 survival analysis was done using the survival R package (Therneau and Grambsch, 2000) (https://cran.r-project.org/web/packages/survival/citation.html). Patients were stratified based on a cg11625005 methylation beta value threshold of 0.75, and differences between the survival curves of the stratified patient groups were tested using the log-rank test. 5mC:C ratios in H3K4me2/3 ChIP of −124 samples were log transformed and compared using a single-sample t test against a hypothetical mean of 1. This analysis assumes that the underlying data are distributed normally. For this analysis, the n was the number of CpGs tested (18) in the *TERT* CGI.

SUPPLEMENTAL INFORMATION

Supplemental Information includes Supplemental Experimental Procedures, four figures, and two tables and can be found with this article online at https://doi.org/10.1016/j.celrep.2017.12.001.

ACKNOWLEDGMENTS

We thank S. Borah (St. Jude's Children's Hospital) and members of the Cech lab for helpful discussion. We thank X. Wang (University of Colorado Boulder) for preparation of PRC2 complexes. We thank F. Lorbeer, C. Kunitoshi, and D. Hockemeyer (University of California, Berkeley) and A. Meeker and S. Yegnasubramanian (Johns Hopkins) for useful conversations relating to this work.

We thank the ENCODE Consortium (Rosenbloom et al., 2013) and the ENCODE production laboratories for generating data used in this study. We thank the Novartis Institute of Biomedical Research for the use of CCLE data. J.L.S. was supported by a postdoctoral fellowship 127621-PF-16-099-01-DMC from the American Cancer Society. F.W.H. was funded by DOD (W81XWH-14-1-0514) and a Prostate Cancer Foundation Young Investigator Award; and T.R.C. is an investigator of the Howard Hughes Medical Institute. This work was funded by NIH grant R01 GM099705 to T.R.C.

AUTHOR CONTRIBUTIONS

J.L.S. designed and performed allele-specific ChIP experiments. J.L.S. and R.D.P. designed and R.D.P. performed PRC2 binding experiments. J.L.S. designed and R.N. performed experiments related to T24 lines. J.L.S. and J.C.C. designed and J.C.C. performed TCGA analyses. F.W.H. and M.G. designed and analyzed CCLE data. J.L.S. and T.R.C. wrote the manuscript.

DECLARATION OF INTERESTS

T.R.C. is on the board of directors of Merck.

Received: July 5, 2017
Revised: September 29, 2017
Accepted: November 30, 2017
Published: December 26, 2017

REFERENCES

Barthel, F.P., Wei, W., Tang, M., Martinez-Ledesma, E., Hu, X., Amin, S.B., Akdemir, K.C., Seth, S., Song, X., Wang, Q., et al. (2017). Systematic analysis of telomere length and somatic alterations in 31 cancer types. Nat. Genet. *49*, 349–357.

Bartke, T., Vermeulen, M., Xhemalce, B., Robson, S.C., Mann, M., and Kouzarides, T. (2010). Nucleosome-interacting proteins regulated by DNA and histone methylation. Cell *143*, 470–484.

Baylin, S.B., Herman, J.G., Graff, J.R., Vertino, P.M., and Issa, J.P. (1998). Alterations in DNA methylation: a fundamental aspect of neoplasia. Adv. Cancer Res. *72*, 141–196.

Bell, R.J.A., Rube, H.T., Kreig, A., Mancini, A., Fouse, S.D., Nagarajan, R.P., Choi, S., Hong, C., He, D., Pekmezci, M., et al. (2015). Cancer. The transcription factor GABP selectively binds and activates the mutant TERT promoter in cancer. Science *348*, 1036–1039.

Borah, S., Xi, L., Zaug, A.J., Powell, N.M., Dancik, G.M., Cohen, S.B., Costello, J.C., Theodorescu, D., and Cech, T.R. (2015). Cancer. TERT promoter mutations and telomerase reactivation in urothelial cancer. Science *347*, 1006–1010.

Castelo-Branco, P., Choufani, S., Mack, S., Gallagher, D., Zhang, C., Lipman, T., Zhukova, N., Walker, E.J., Martin, D., Merino, D., et al. (2013). Methylation of the TERT promoter and risk stratification of childhood brain tumours: an integrative genomic and molecular study. Lancet Oncol. *14*, 534–542.

Castelo-Branco, P., Leão, R., Lipman, T., Campbell, B., Lee, D., Price, A., Zhang, C., Heidari, A., Stephens, D., Boerno, S., et al. (2016). A cancer specific hypermethylation signature of the TERT promoter predicts biochemical relapse in prostate cancer: a retrospective cohort study. Oncotarget *7*, 57726–57736.

Cedar, H., and Bergman, Y. (2009). Linking DNA methylation and histone modification: patterns and paradigms. Nat. Rev. Genet. *10*, 295–304.

Counter, C.M., Avilion, A.A., LeFeuvre, C.E., Stewart, N.G., Greider, C.W., Harley, C.B., and Bacchetti, S. (1992). Telomere shortening associated with chromosome instability is arrested in immortal cells which express telomerase activity. EMBO J. *11*, 1921–1929.

Dessain, S.K., Yu, H., Reddel, R.R., Beijersbergen, R.L., and Weinberg, R.A. (2000). Methylation of the human telomerase gene CpG island. Cancer Res. *60*, 537–541.

Devereux, T.R., Horikawa, I., Anna, C.H., Annab, L.A., Afshari, C.A., and Barrett, J.C. (1999). DNA methylation analysis of the promoter region of the human telomerase reverse transcriptase (hTERT) gene. Cancer Res. *59*, 6087–6090.

Epsztejn-Litman, S., Feldman, N., Abu-Remaileh, M., Shufaro, Y., Gerson, A., Ueda, J., Deplus, R., Fuks, F., Shinkai, Y., Cedar, H., and Bergman, Y. (2008). De novo DNA methylation promoted by G9a prevents reprogramming of embryonically silenced genes. Nat. Struct. Mol. Biol. *15*, 1176–1183.

Fan, Y., Lee, S., Wu, G., Easton, J., Yergeau, D., Dummer, R., Vogel, P., Kirkwood, J.M., Barnhill, R.L., Pappo, A., and Bahrami, A. (2016). Telomerase expression by aberrant methylation of the TERT promoter in melanoma arising in giant congenital nevi. J. Invest. Dermatol. *136*, 339–342.

Gildea, J.J., Golden, W.L., Harding, M.A., and Theodorescu, D. (2000). Genetic and phenotypic changes associated with the acquisition of tumorigenicity in human bladder cancer. Genes Chromosomes Cancer *27*, 252–263.

Gildea, J.J., Seraj, M.J., Oxford, G., Harding, M.A., Hampton, G.M., Moskaluk, C.A., Frierson, H.F., Conaway, M.R., and Theodorescu, D. (2002). RhoGDI2 is an invasion and metastasis suppressor gene in human cancer. Cancer Res. *62*, 6418–6423.

Gojo, J., Lötsch, D., Spiegl-Kreinecker, S., Pajtler, K.W., Neumayer, K., Korbel, P., Araki, A., Brandstetter, A., Mohr, T., Hovestadt, V., et al. (2017). Telomerase activation in posterior fossa group A ependymomas is associated with dismal prognosis and chromosome 1q gain. Neuro Oncol. *19*, 1183–1194.

Greer, E.L., and Shi, Y. (2012). Histone methylation: a dynamic mark in health, disease and inheritance. Nat. Rev. Genet. *13*, 343–357.

Guilleret, I., and Benhattar, J. (2004). Unusual distribution of DNA methylation within the hTERT CpG island in tissues and cell lines. Biochem. Biophys. Res. Commun. *325*, 1037–1043.

Herman, J.G. (1999). Hypermethylation of tumor suppressor genes in cancer. Semin. Cancer Biol. *9*, 359–367.

Herman, J.G., Umar, A., Polyak, K., Graff, J.R., Ahuja, N., Issa, J.P., Markowitz, S., Willson, J.K., Hamilton, S.R., Kinzler, K.W., et al. (1998). Incidence and functional consequences of hMLH1 promoter hypermethylation in colorectal carcinoma. Proc. Natl. Acad. Sci. USA *95*, 6870–6875.

Horn, S., Figl, A., Rachakonda, P.S., Fischer, C., Sucker, A., Gast, A., Kadel, S., Moll, I., Nagore, E., Hemminki, K., et al. (2013). TERT promoter mutations in familial and sporadic melanoma. Science *339*, 959–961.

Huang, F.W., Hodis, E., Xu, M.J., Kryukov, G.V., Chin, L., and Garraway, L.A. (2013). Highly recurrent TERT promoter mutations in human melanoma. Science *339*, 957–959.

Huang, F.W., Bielski, C.M., Rinne, M.L., Hahn, W.C., Sellers, W.R., Stegmeier, F., Garraway, L.A., and Kryukov, G.V. (2015). TERT promoter mutations and monoallelic activation of TERT in cancer. Oncogenesis *4*, e176.

Killela, P.J., Reitman, Z.J., Jiao, Y., Bettegowda, C., Agrawal, N., Diaz, L.A., Jr., Friedman, A.H., Friedman, H., Gallia, G.L., Giovanella, B.C., et al. (2013). TERT promoter mutations occur frequently in gliomas and a subset of tumors derived from cells with low rates of self-renewal. Proc. Natl. Acad. Sci. USA *110*, 6021–6026.

Laird, P.W., and Jaenisch, R. (1996). The role of DNA methylation in cancer genetic and epigenetics. Annu. Rev. Genet. *30*, 441–464.

Lindsey, J.C., Schwalbe, E.C., Potluri, S., Bailey, S., Williamson, D., and Clifford, S.C. (2014). TERT promoter mutation and aberrant hypermethylation are associated with elevated expression in medulloblastoma and characterise the majority of non-infant SHH subgroup tumours. Acta Neuropathol. *127*, 307–309.

Liu, X., Gao, Q., Li, P., Zhao, Q., Zhang, J., Li, J., Koseki, H., and Wong, J. (2013). UHRF1 targets DNMT1 for DNA methylation through cooperative binding of hemi-methylated DNA and methylated H3K9. Nat. Commun. *4*, 1563.

Lynch, M.D., Smith, A.J.H., De Gobbi, M., Flenley, M., Hughes, J.R., Vernimmen, D., Ayyub, H., Sharpe, J.A., Sloane-Stanley, J.A., Sutherland, L., et al. (2012). An interspecies analysis reveals a key role for unmethylated CpG dinucleotides in vertebrate Polycomb complex recruitment. EMBO J. *31*, 317–329.

Maunakea, A.K., Nagarajan, R.P., Bilenky, M., Ballinger, T.J., D'Souza, C., Fouse, S.D., Johnson, B.E., Hong, C., Nielsen, C., Zhao, Y., et al. (2010).

Conserved role of intragenic DNA methylation in regulating alternative promoters. Nature *466*, 253–257.

McGarvey, K.M., Fahrner, J.A., Greene, E., Martens, J., Jenuwein, T., and Baylin, S.B. (2006). Silenced tumor suppressor genes reactivated by DNA demethylation do not return to a fully euchromatic chromatin state. Cancer Res. *66*, 3541–3549.

Merlo, A., Herman, J.G., Mao, L., Lee, D.J., Gabrielson, E., Burger, P.C., Baylin, S.B., and Sidransky, D. (1995). 5′ CpG island methylation is associated with transcriptional silencing of the tumour suppressor p16/CDKN2/MTS1 in human cancers. Nat. Med. *1*, 686–692.

Mozzetta, C., Boyarchuk, E., Pontis, J., and Ait-Si-Ali, S. (2015). Sound of silence: the properties and functions of repressive Lys methyltransferases. Nat. Rev. Mol. Cell Biol. *16*, 499–513.

Neri, F., Rapelli, S., Krepelova, A., Incarnato, D., Parlato, C., Basile, G., Maldotti, M., Anselmi, F., and Oliviero, S. (2017). Intragenic DNA methylation prevents spurious transcription initiation. Nature *543*, 72–77.

Pfister, S.X., and Ashworth, A. (2017). Marked for death: targeting epigenetic changes in cancer. Nat. Rev. Drug Discov. *16*, 241–263.

Rose, N.R., and Klose, R.J. (2014). Understanding the relationship between DNA methylation and histone lysine methylation. Biochim. Biophys. Acta *1839*, 1362–1372.

Rosenbloom, K.R., Sloan, C.A., Malladi, V.S., Dreszer, T.R., Learned, K., Kirkup, V.M., Wong, M.C., Maddren, M., Fang, R., Heitner, S.G., et al. (2013). ENCODE data in the UCSC Genome Browser: year 5 update. Nucleic Acids Res. *41*, D56–D63.

Rothbart, S.B., Krajewski, K., Nady, N., Tempel, W., Xue, S., Badeaux, A.I., Barsyte-Lovejoy, D., Martinez, J.Y., Bedford, M.T., Fuchs, S.M., et al. (2012). Association of UHRF1 with methylated H3K9 directs the maintenance of DNA methylation. Nat. Struct. Mol. Biol. *19*, 1155–1160.

Rothbart, S.B., Dickson, B.M., Ong, M.S., Krajewski, K., Houliston, S., Kireev, D.B., Arrowsmith, C.H., and Strahl, B.D. (2013). Multivalent histone engagement by the linked tandem Tudor and PHD domains of UHRF1 is required for the epigenetic inheritance of DNA methylation. Genes Dev. *27*, 1288–1298.

Schübeler, D. (2015). Function and information content of DNA methylation. Nature *517*, 321–326.

Seynnaeve, B., Lee, S., Borah, S., Park, Y., Pappo, A., Kirkwood, J.M., and Bahrami, A. (2017). Genetic and epigenetic alterations of TERT are associated with inferior outcome in adolescent and young adult patients with melanoma. Sci. Rep. *7*, 45704.

Smith, Z.D., and Meissner, A. (2013). DNA methylation: roles in mammalian development. Nat. Rev. Genet. *14*, 204–220.

Stern, J.L., Theodorescu, D., Vogelstein, B., Papadopoulos, N., and Cech, T.R. (2015). Mutation of the TERT promoter, switch to active chromatin, and monoallelic TERT expression in multiple cancers. Genes Dev. *29*, 2219–2224.

Therneau, T.M., and Grambsch, P.M. (2000). Modeling survival data: Extending the Cox Model (Springer, New York).

Wang, X., Paucek, R.C., Gooding, A.R., Brown, Z.Z., Ge, E.J., Muir, T.W., and Cech, T.R. (2017). PRC2 recruitment to DNA in chromatin and its inhibition by RNA reveal molecular mechanisms of epigenetic control. Nat. Struct. Mol. Biol. Published online October 26, 2017. https://doi.org/10.1038/nsmb.3487.

Cell Reports, Volume *21*

Supplemental Information

Allele-Specific DNA Methylation and Its Interplay with Repressive Histone Marks at Promoter-Mutant *TERT* Genes

Josh Lewis Stern, Richard D. Paucek, Franklin W. Huang, Mahmoud Ghandi, Ronald Nwumeh, James C. Costello, and Thomas R. Cech

Supplemental Experimental Procedures

RESOURCE TABLE

REAGENT or RESOURCE	SOURCE	IDENTIFIER
Antibodies		
H3K4me2/3	Abcam	ab-6000
H3K27me3	EMD Millipore	07-449
EZH2	Active Motif	ac22
H3K9me3	EMD Millipore	07-442
IgG control	EMD Millipore	12-370
Critical Commercial Assays		
EZ DNA methylation-Gold Kit	Zymo Research	D5005
IQ SYBR Green Supermix	Biorad	1708880
7-Deaza-2'-deoxy-guanosine-5'-triphosphate	Roche	10988537001
SYBRselect	ThermoFisher	4472919
pGEM®-T Easy Vector	Promega	A1360
Superscript III	ThermoFisher	18080-044
Experimental Models: Cell Lines		
SNU-475	ATCC	CRL-2236
SNU-423	ATCC	CRL-2238
Human fibroblasts	ATCC	PCS-201-012
WM793	Wistar Institute	WM793
HepG2	ATCC	HB-8065
U87MG, SK-N-SH, SCaBER, T24 and related lines	University of Colorado, Anschutz Cancer Center Protein Production Shared Resource	U87MG, SCaBER , T24, T24T, FL3, SLT4
See Table S1 for CCLE cell lines.		
Oligonucleotides		
Bisulfite *TERT* CGI Forward 5’- TTTGAGAATTTGTAAAGAGAAATGA-3’	IDT	
Bisulfite *TERT* CGI Reverse 5’-AATATAAAAACCCTAAAAACAAATAC-3’	IDT	
Bisulfite CpG 1-8 sequencing 5’-AAACTAAAAAATAAAAAAACAAAAC-3’	IDT	
Bisulfite CpG 9-18 sequencing 5’- ATATAAAAACCCTAAAAACAAATAC-3’		
EMSA top strand 5’-AATGCGTCCTCGGGTTCGTCCCCAGCCGCGTCTACGCGCCTCCGTCCT - 3’	IDT	
EMSA bottom 5’-AGGACGGAGGCGCGTAGACGCGGCTGGGGACGAACCCGAGGACGCATT - 3’	IDT	
TERT Exon 14 Foward 5’-CATTTCATCAGCAAGTTTGGAAG-3’	IDT	
TERT Exon 14 Reverse 5’-TTTCAGGATGGAGTAGCAGAGG-3’	IDT	
Random Hexamer	ThermoFisher	N8080127
qPCR primer spanning cg11625005 Forward 5’-CTGTGTCAAGGAGCCCAAGT -3’	IDT	
qPCR primer spanningcg11625005 Reverse 5’-CTGGCCTGATCCGGAGAC -3′	IDT	
qPCR primer between cg11625005 and -124 mutation Forward 5’-CGTCCTCCCCTTCACGTC -3’	IDT	

qPCR primer between cg11625005 and -124 mutation Reverse 5'-GCCTAGGCTGTGGGGTAAC -3′	IDT	
qPCR primer spanning -124 mutation Forward 5'-GTCCTGCCCCTTCACCTT-3'	IDT	
qPCR primer spanning -124 mutation Reverse 5'-AGCGCTGCCTGAAACTCG-3′	IDT	
Software and Algorithms		
MethPrimer	(Li and Dahiya, 2002)	http://www.urogene.org/cgi-bin/methprimer/methprimer.cgi
Snapgene viewer		http://www.snapgene.com/products/snapgene_viewer/
cBioPortal for TCGA	(Cerami et al., 2012; Gao et al., 2013)	http://www.cbioportal.org/data_sets.jsp
R	(Therneau, 1999)	https://www.r-project.org/
Other		
Protein G/Protein A agarose beads	EMD Millipore	IP05-1.5 mL
Protease inhibitor Cocktail	ThermoFisher-Pierce	88266
MinElute gel extraction kit	Qiagen	28606
RNase A	ThermoFischer	am2272
HiTrap Heparin column	GE	17-0407-03
RQ1 DNase	Promega	M6101
Amicon Ultra-15 Centrifugal Filter Unit, 30 kDa molecular weight cut-off	Millipore	UFC903024

Chromatin Immunoprecipitation, Bisulfite Conversion and PCR

ChIP was performed as previously described (Stern et al., 2015). For immunoprecipitation, 5-25 µg of solubilized chromatin was used with 2-4 µg of α-H3K4me2/3 (Abcam, ab-6000), α-H3K27me3 (EMD Millipore, 07-449), α-EZH2 (ac22) (Active Motif), α -H3K9me3 (07-442, EMD Millipore) or a non-specific IgG control (12-370, EMD Millipore) of equal mass, and nutated overnight at 4°C. Protein G/Protein A agarose beads (IP05-1.5 mL, EMD Millipore Corporation) were added for three hours and then treated as previously described (Stern et al., 2015). Bisulfite conversion of ChIP-purified material was performed using the EZ DNA Methylation-Gold Kit (D5005, Zymo).

CCLE Methylation Analysis

Cell lines from the CCLE underwent reduced RRBS as previously described (Landau et al., 2014). RNAseq data and *TERT* promoter mutations were annotated as previously described (Huang et al., 2015). A total of 278 lines were analyzed for which the *TERT* promoter mutation status, RNAseq data, and methylation data at the *TERT* locus were determined.

EMSA and PRC2-5mC-DNA Binding

5mC substituted DNA was synthesized by Integrated DNA technologies. All DNA substrates were radiolabeled using T4 PNK (NEB M0201L) by standard protocol. Stock PRC2 was diluted in binding buffer and added to radiolabeled DNA. The binding reaction was carried out for 30 min at 30°C, followed by loading samples onto non-denaturing 1.0% native agarose gel (Fisher BP160-100) buffered with TRIS/borate/EDTA (TBE) at 4°C. Dried gels were exposed to phosphorimaging plates, which were scanned using a Typhoon Trio phosphorimager (GE Healthcare) for signal acquisition. Gel analysis was carried out with ImageQuant software (GE Healthcare) and data fitted to a sigmoidal binding curve using MATLAB (MathWorks).

Cell Culture

SNU-423, SNU-475, HepG2 were obtained from American Type Culture Collection. U87MG, SK-N-SH, SCaBER, T24, T24T, FL3, SLT4, obtained from the University of Colorado, Anschutz, Tissue Culture Shared Resource. WM793 cells were obtained from S. Spencer at the University of Colorado, Boulder. All cells were cultured in DMEM (VWR Scientific) with

2mM GlutaminePlus (Atlanta Biologicals), 10% FBS (Thermo Fisher), 2 mM GlutaMAX-I (GIBCO), 100 units/ml penicillin and 100 mg/ml streptomycin (GIBCO) and 1mM sodium pyruvate (GIBCO), except U87MG and HepG2 cells were cultured in EMEM (American Type Culture Collection) plus serum and glutamxax, but without sodium pyruvate.

RNA Extraction and cDNA Preparation

Following RNA extraction with Trizol (Life Technologies), reverse transcription was performed by treating of 10 µg of RNA with 5 U of RQ1 DNase (Promega) according to the manufacturer's protocol, followed by phenol extraction (pH 7), chloroform:isoamyl alcohol extraction, and then ethanol precipitation. The cDNA was generated from 2 µg of RNA synthesized using random hexamers, oligo(dT) 20-mer, and SuperScript III (Life Technologies). Following treatment with RNase H (New England Biolabs) quantitative PCR was performed with either SybrSelect (Thermo Fisher) or iQ SYBR Green (Bio-Rad) PCR mix using a Roche LightCycler 480 with the program 10 min at 98°C, 30 sec at 95°C, 30 sec at 60°C, 30 sec at 72°C, and 5 min at 72°C, followed by quantification using the Roche LightCycler 480 software. Melt curve analyses were examined to ensure the uniformity of relevant PCR amplicons and all PCR amplicons were sequenced at least once to confirm the product identity. Primers for TERT mRNA exon 2 were forward 5'-CGTGGTTTCTGTGTGGTGTC-3, reverse 5'-CCTTGTCGCCTGAGGAGTAG-3'; and exon 14 were those previously described (Borah et al., 2015).

TERT CpG island coordinates were assessed using the UCSC Genome Browser bona fide CpG island data (Bock et al., 2007). This CGI island is commonly analyzed using the Infinium 450K BeadChip methylation arrays from Illumina which contains a probe (cg11625005) for this region that is designed to hybridized to the 50 bases preceding the chr5:1295737 (HG19). This probe on the Infinium arrays reports on the methylation status of this CpG dinucleotide.

Bisulfite ChIP Analysis

PCR with bisulfite converted samples was performed using BioRad iQ SYBR Green PCR mix using the program: 10 min at 95°C, followed by 17 step-down cycles of 1 min at 95°C, 1 min at 70°C–54° C, and 2 min at 72°C; 30 cycles of 1 min at 95°C, 1 min at 56°C, and 2 min at 72°C; and 10 min at 72°C. Temperature ramp rates for primer annealing were 1°C/min and extension at 2°C/min. Bisulfite primer sequences for amplifying the region of the *TERT* CGI were designed using MethPrimer (http://www.urogene.org/cgi-bin/methprimer/methprimer.cgi) and were forward 5'-TTTGAGAATTTGTAAAGAGAAATGA-3'; revervse 5'AATATAAAAACCCTAAAAACAAATAC-3'; and sequenced using 5'-AAACTAAAAAATAAAAAAACAAAAC-3' for CpGs 1-8 and 5'ATATAAAAACCCTAAAAACAAATAC-3' for CpGs 9-18. Three PCR reactions were pooled for each sample, and gel purified (Qiagen miniElute) followed by sequencing (Genewiz). Sequencing analysis was performed using Snapgene and Sequence Scanner 2.0 (Applied Biosystems). To account for non-normal distribution of peak heights, data were log transformed prior to taking averages, and then back-transformed to calculate ratios for ChIP/input values.

cg11625005 Survival Analysis

The methylation data for patients with samples run on the Illumina Human Methylation 450 arrays are reported in the associated TCGA studies. Beta values for cg11625005 were extracted from the associated patient files, and the average was calculated for any patient that had data generated for multiple vials according to the TCGA barcode. Patients were stratified based on a methylation beta value threshold of 0.75 and differences between the survival curves of the stratified patient groups were tested using the log-rank test. The results in this study are in whole or part based upon data generated by the TCGA Research Network: http://cancergenome.nih.gov/. Processed files with computed methylation beta values were downloaded from the Genomic Data Commons (https://gdc.cancer.gov/). Clinical information, including overall survival (OS_STATUS and OS_MONTHS) was downloaded from cBioPortal (Cerami et al., 2012) under the bulk data download (http://www.cbioportal.org/data_sets.jsp). All datasets (BLCA, BRCA, CESC, GBM, HNSC, LGG, LIHC, LUAD, LUSC, PRAD, SKCM, THCA) were processed through cBioPortal on June 22, 2016.

EZH2 Survival Analysis for Primary Tumors

Gene expression profiles for EZH2 and overall survival information were selected for patients in the TCGA (SKCM, LIHC, STAD, KIRP) using the CGDS-R R package (v1.2.5; https://github.com/cBioPortal/cgdsr). Each cancer type was filtered to only include primary tumor samples. To find the gene expression threshold that defined the best overall patient survival stratification, EZH2 expression values were ranked, then patients were iteratively stratified into low and high EZH2

expression groups. Overall survival comparisons between these two groups were made using the log rank test in the R survival package (v 2.40-1; https://github.com/therneau/survival). The EZH2 expression value that resulted in the most significant patient stratification defined the best separation threshold and was used for plotting overall patient survival.

Protein Expression and Purification

Human PRC2 5-mer complexes were expressed in insect cells as previously described (Davidovich et al., 2013; Wang et al., 2017). In brief, sequences encoding human EZH2, SUZ12, EED, RBBP4, and AEBP2 were cloned into the pfast-bac1 expression vector (Invitrogen) with PreScission-cleavable N-terminal hexahistidine-MBP tags. Standard Bac-to-Bac baculovirus expression system (Invitrogen) was used to generate baculovirus stocks according to manufacturer's protocol. Following infection, the cells were incubated for 72 h (27°C, 130 rpm) before they were harvested. The harvested cells were snap-frozen for later purification. PRC2 was purified as previously described (Wang et al., 2017). In brief, cell extract was incubated with the amylose resin and washed thoroughly, followed by elution with 10 mM maltose. The eluate was concentrated, then followed by digestion with PreScission protease at a mass ratio of 1:50 protease:protein. After completion of cleavage, protein complex was injected into a 5 mL Hi-Trap Heparin column (GE, 17-0407-03), followed by fractionation over a HiPrep 16/60 Sephacryl S-400 HR sizing column. PRC2 peak fractions were identified using SDS-PAGE, pooled, and concentrated as above. Final protein concentration was measured by absorbance at 280 nm, and the ratio of absorbance at 260 nm/280 nm was <0.7, an indication of no nucleic acid contamination.

EMSA and PRC2-5mC-DNA Binding

5mC substituted DNA was synthesized by Integrated DNA technologies. All DNA substrates were radiolabeled using T4 PNK (NEB M0201L) by standard protocol. After labeling, excess [γ-32P]-ATP in the reaction was removed by running the samples over a G50 Sephadex column (Roche 11 273 949 001). Radiolabeled DNA substrates were purified by native polyacrylamide gel electrophoresis (PAGE). DNA was extracted and pellets were dissolved in TRIS-EDTA buffer, pH 7.5. The radiolabeling efficiency of the purified DNA was determined by liquid scintillation counting. Radiolabeled DNA, with specific activity no less than 100,000 cpm/pmol, was adjusted with binding buffer (50 mM Tris-HCl pH 7.5 at 25°C, 100 mM KCl, 2.5 mM MgCl2, 0.1 mM ZnCl2, 2 mM 2-mercaptoethanol, 0.05% v/v NP-40, 0.1 mg/ml bovine serum albumin, 5% v/v glycerol). Next, stock PRC2 was diluted in binding buffer and added to radiolabeled DNA. The binding reaction was carried out for 30 min at 30°C, followed by loading samples onto non-denaturing 1.0% native agarose gel (Fisher BP160-100) buffered with TRIS/borate/EDTA (TBE) at 4°C. Gel electrophoresis was carried out for 90 min at 66 V packed in an ice box within a 4°C cold room. A Hybond N+membrane (Amersham, Fisher Scientific 45-000-927) and two sheets of Whatman 3 mm chromatography paper were put underneath the gel, which then was vacuum dried for 60 min at 80°C. Dried gels were exposed to phosphorimaging plates, which were scanned using a Typhoon Trio phosphorimager (GE Healthcare) for signal acquisition. Gel analysis was carried out with ImageQuant software (GE Healthcare) and data fitted to a sigmoidal binding curve using MATLAB (MathWorks).

References

Borah, S., Xi, L., Zaug, A.J., Powell, N.M., Dancik, G.M., Cohen, S.B., Costello, J.C., Theodorescu, D., and Cech, T.R. (2015). TERT promoter mutations and telomerase reactivation in urothelial cancer. Science. *347*, 1006–1010.

Cerami, E., Gao, J., Dogrusoz, U., Gross, B.E., Sumer, S.O., Aksoy, B.A., Jacobsen, A., Byrne, C.J., Heuer, M.L., Larsson, E., et al. (2012). The cBio Cancer Genomics Portal: An open platform for exploring multidimensional cancer genomics data. Cancer Discov. *2*, 401–404.

Gao, J., Arman Aksoy, B., Dogrusoz, U., Dresdner, G., Gross, B., Sumer, S.O., Sun, Y., Jacobsen, A., Sinha, R., Larsson, E., et al. (2013). Integrative analysis of complex cancer genomics and clinical Profiles Using the cBioPortal Performing cross-cancer Queries Viewing cancer Study Summary Data Viewing genomic alterations in a Single Tumor. Sci. Signal. *6*, 1–2.

Huang, F.W., Bielski, C.M., Rinne, M.L., Hahn, W.C., Sellers, W.R., Stegmeier, F., Garraway, L.A., and Kryukov, G. V (2015). TERT promoter mutations and monoallelic activation of TERT in cancer. Oncogenesis *4*, e176.

Landau, D.A., Clement, K., Ziller, M.J., Boyle, P., Fan, J., Gu, H., Stevenson, K., Sougnez, C., Wang, L., Li, S., et al. (2014). Locally Disordered Methylation Forms the Basis of Intratumor Methylome Variation in Chronic Lymphocytic Leukemia. Cancer Cell *26*, 813–825.

Li, L.-C., and Dahiya, R. (2002). MethPrimer: designing primers for methylation PCRs. Bioinformatics *18*, 1427–1431.

Stern, J., Theodorescu, D., Vogelstein, B., Papadopoulos, N., and Cech, T.R. (2015). Mutation of the TERT promoter, switch to active chromatin, and monoallelic TERT expression in multiple cancers. Genes Dev *29*, 2219–2224.

Therneau, T.M. (1999). A Package for Survival Analysis in S. Mayo Clin. Found. 70–73.

Figure S1.

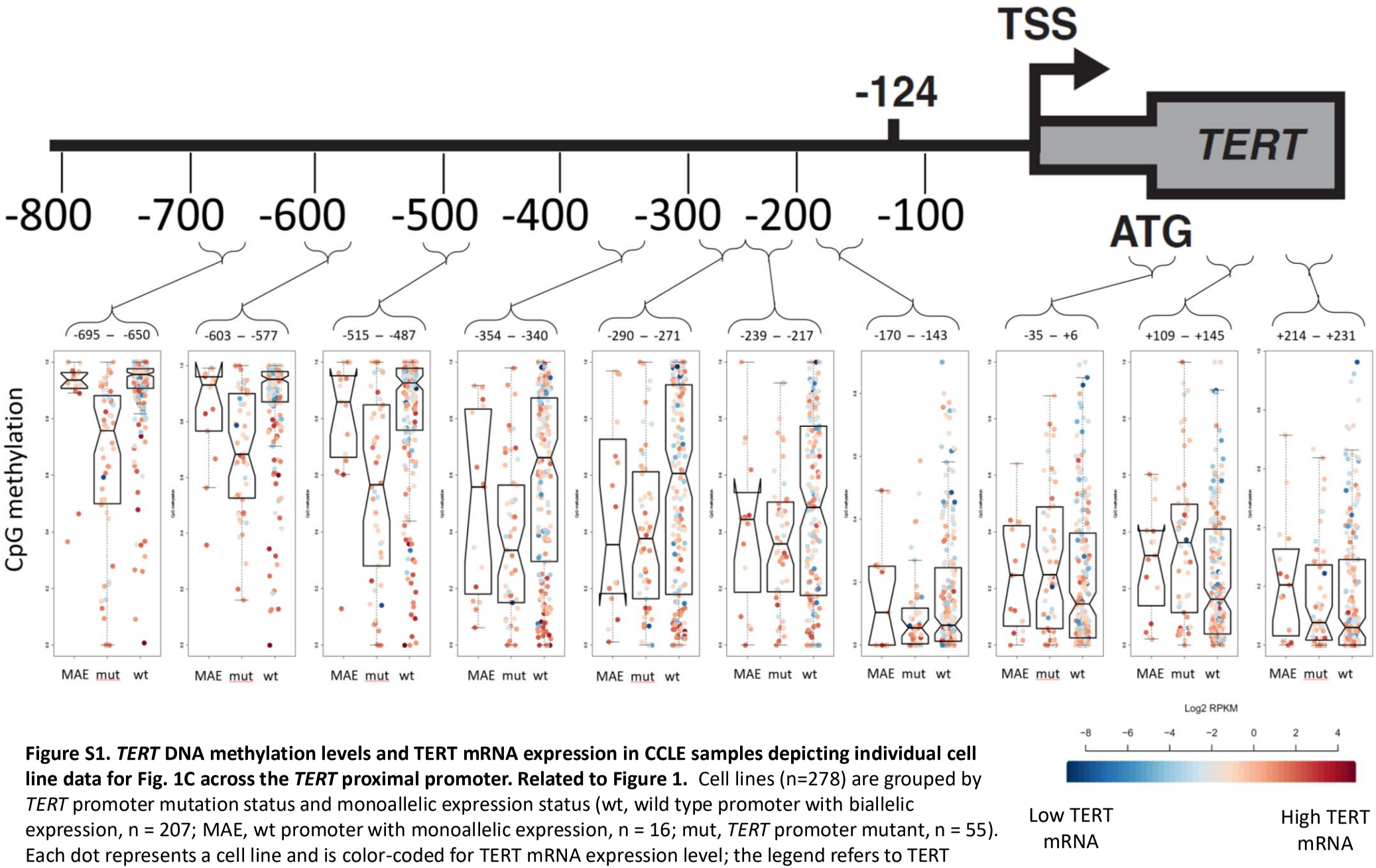

Figure S1. *TERT* DNA methylation levels and TERT mRNA expression in CCLE samples depicting individual cell line data for Fig. 1C across the *TERT* proximal promoter. Related to Figure 1. Cell lines (n=278) are grouped by *TERT* promoter mutation status and monoallelic expression status (wt, wild type promoter with biallelic expression, n = 207; MAE, wt promoter with monoallelic expression, n = 16; mut, *TERT* promoter mutant, n = 55). Each dot represents a cell line and is color-coded for TERT mRNA expression level; the legend refers to TERT mRNA levels where blue refers to lower TERT mRNA levels, red indicates higher TERT mRNA. Each boxplot displays the median methylation level and 1st and 3rd quartiles. Tests for significance between wt and -124/-146 are displayed in Fig. 1C and in Table S2.

Figure S2.

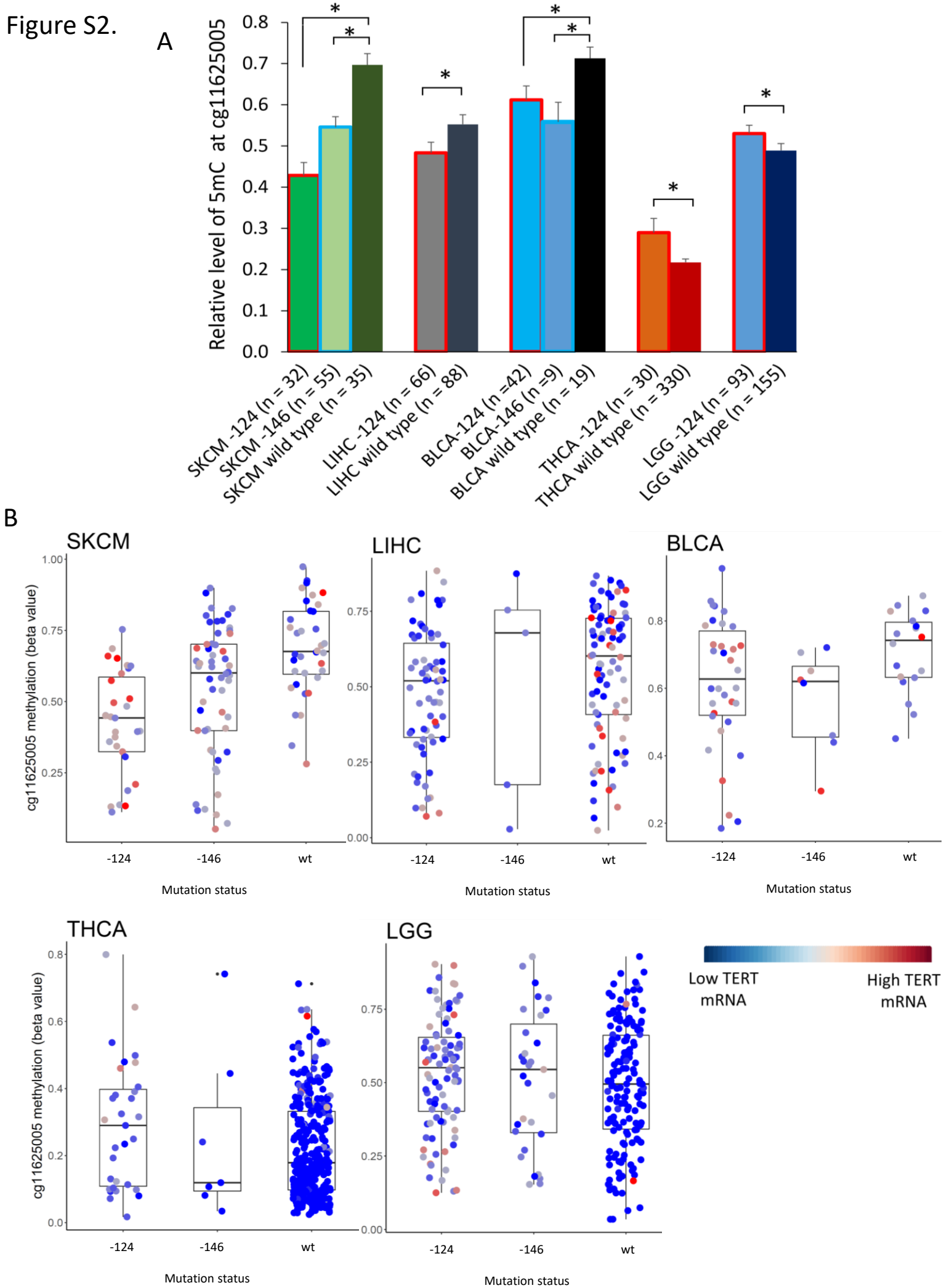
A
Relative level of 5mC at cg11625005
0.0
0.1
0.2
0.3
0.4
0.5
0.6
0.7
0.8
*
SKCM -124 (n = 32)
SKCM -146 (n = 55)
SKCM wild type (n = 35)
LIHC -124 (n = 66)
LIHC wild type (n = 88)
BLCA-124 (n =42)
BLCA-146 (n =9)
BLCA wild type (n = 19)
THCA -124 (n = 30)
THCA wild type (n = 330)
LGG -124 (n = 93)
LGG wild type (n = 155)
B
SKCM
LIHC
BLCA
THCA
LGG
cg11625005 methylation (beta value)
-124
-146
wt
Mutation status
Low TERT mRNA
High TERT mRNA

Figure S2. 5mC Levels at cg11625005 in Patient Tumor Samples with *vs.* without *TERT* Promoter Mutations. Related to Figure 1. (A) Reduced methylation at cg11625005 in -124 and -146 mutant *TERT* promoters in TCGA patient tumor samples. Melanoma, SKCM; LIHC, liver cancer; BLCA, bladder cancer; THCA, thyroid cancer; LGG, lower grade glioma; n = the number of patient samples in each group. Error bars are +SEM. BLCA, $p < 0.05$ for both -124 and -146 mutants; SKCM, $p < 0.001$ for -124 mutants, $p < 0.05$ for -146 mutants; LIHC, $p < 0.05$; THCA $p < 0.02$; LGG $p < 0.0001$. P values were generated using an unpaired, two-tailed t-test assuming equal variance. (B) In cancers that commonly exhibit -124 mutations, 5mC did not correlate with TERT mRNA expression. Where sufficient data were available, TCGA samples were assigned a status for the -124 mutation and RNAseq data were analyzed. BLCA, bladder cancer; LGG, lower grade glioma; LIHC, liver hepatocellular carcinoma; SKCM, cutaneous melanoma; THCA, thyroid cancer. TERT mRNA levels are color coded; blue refers to lower TERT mRNA levels, red refers to higher TERT mRNA levels. Each dot represents a single patient sample.

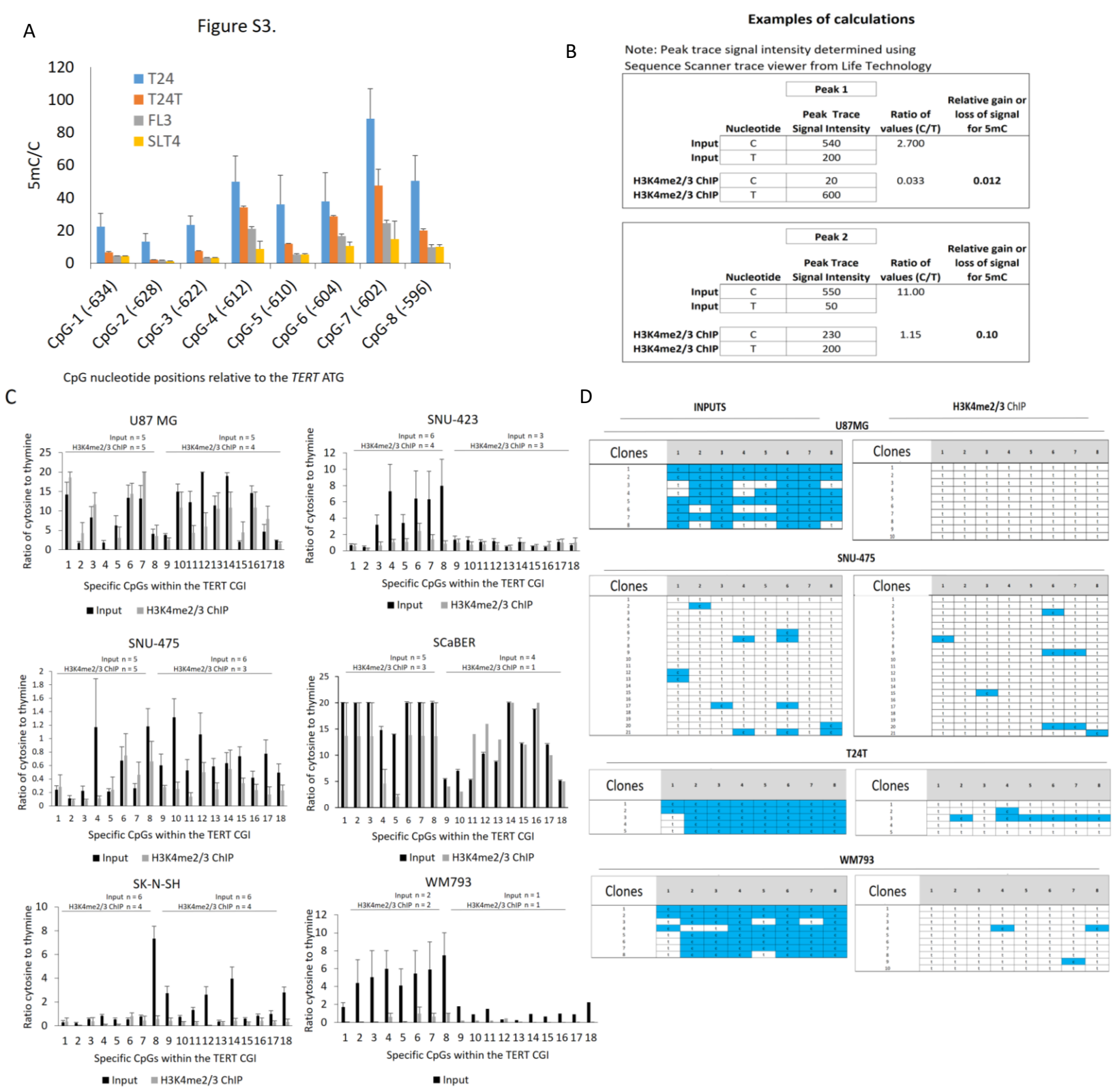

Figure S3. Bisulfite sequencing data for heterozygous cell lines. Related to Figure 2. (A) 5mC in the *TERT* CGI in T24 and related lines. Data are mean 5mC/cystosine ratios for specific CpGs (see Fig. 3D) +SEM; n = 4. T24 bladder carcinoma cells are a -124 mutant, non-metastatic tumor-derived cell line; T24T is a metastatic relative of T24 and was subsequently passaged through mice to obtain the metastatic lines FL3 and SLT4 (Gildea *et al*., 2000, 2002). (B) Example of a calculation to determine sequencing ratios of peak heights for bisulfite converted DNA samples in bisulfite PCR products. (C) Allele-specific H3K4me2/3 ChIP bisulfite sequencing data for individual heterozygous cell lines. Data are the ratio of the peak heights of cytosines to thymine. Data are untransformed means + SEM. Number of biological replicates (n) are indicated above bars. (D) T/A cloned PCR products from bisulfite converted PCR products generated from input and H3K4me2/3 ChIP samples in U87MG glioblastoma, liver cancer line SNU- 475, bladder cancer line T24T, and the melanoma line WM793. Data are for CpGs 1-8 as detailed in Figure 2. c = cytosine, t = thymine. The presence of a c indicates protection from bisulfite conversion due to the presence of 5mC.

Figure S4.

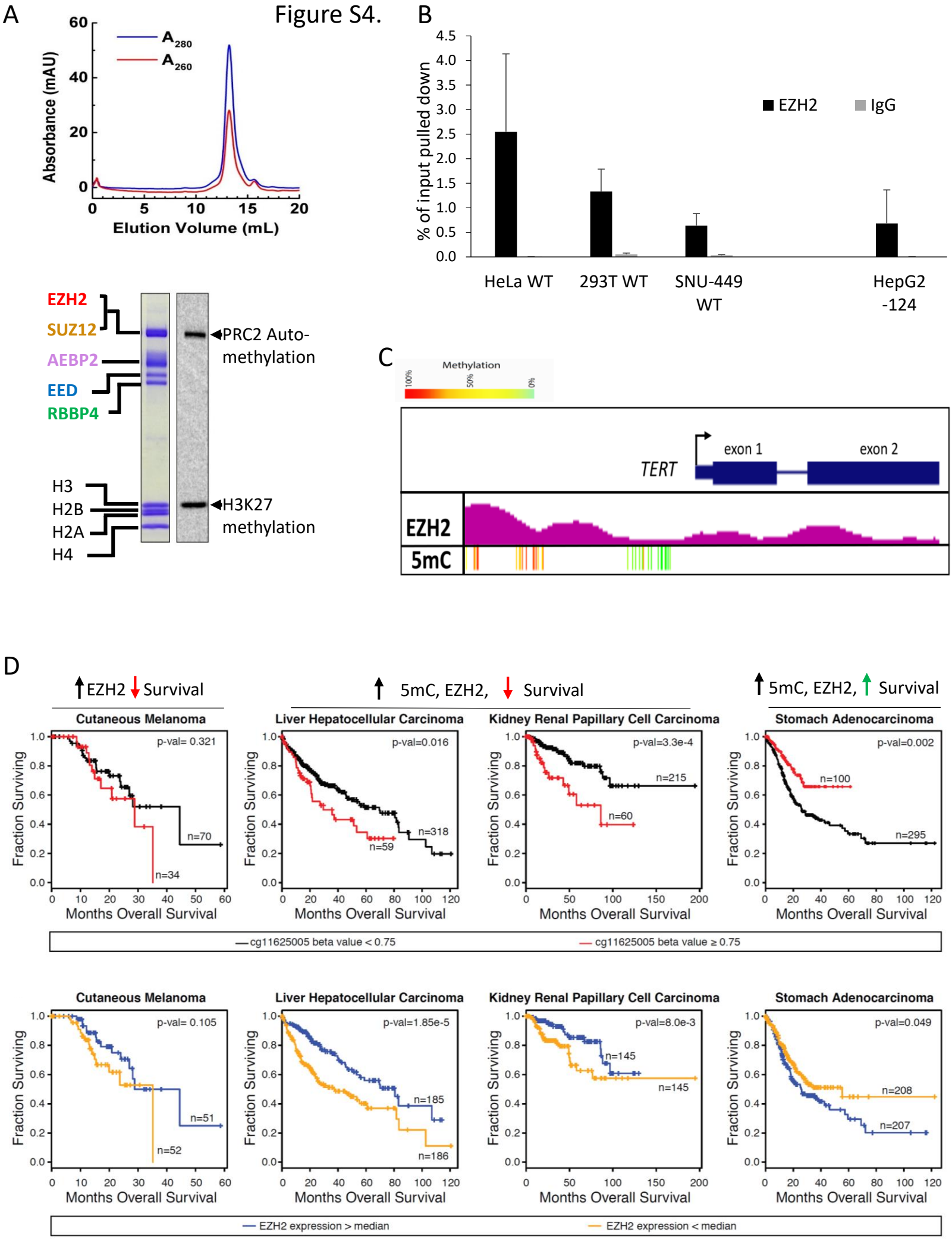
A
Absorbance (mAU)
Elution Volume (mL)
A280
A260
EZH2
SUZ12
AEBP2
EED
RBBP4
H3
H2B
H2A
H4
PRC2 Auto-methylation
H3K27 methylation
B
% of input pulled down
EZH2
IgG
HeLa WT
293T WT
SNU-449 WT
HepG2 -124
C
Methylation
100%
50%
0%
TERT
exon 1
exon 2
EZH2
5mC
D
EZH2 Survival
5mC, EZH2, Survival
5mC, EZH2, Survival
Cutaneous Melanoma
Liver Hepatocellular Carcinoma
Kidney Renal Papillary Cell Carcinoma
Stomach Adenocarcinoma
Fraction Surviving
Months Overall Survival
p-val= 0.321
p-val=0.016
p-val=3.3e-4
p-val=0.002
n=70
n=34
n=318
n=59
n=215
n=60
n=100
n=295
cg11625005 beta value < 0.75
cg11625005 beta value ≥ 0.75
p-val= 0.105
p-val=1.85e-5
p-val=8.0e-3
p-val=0.049
n=51
n=52
n=185
n=186
n=145
n=145
n=208
n=207
EZH2 expression > median
EZH2 expression < median

Figure S4. Relationship between EZH2 and 5mC at the *TERT* promoter. Related to Figure 3. (A) Relates to Fig 3D-F. Top, PRC2 is monodisperse by size-exclusion chromatography on a Superose 6 Increase column. The absence of nucleic acid contamination is indicated by absorbance ratio 260/280 < 0.7. Bottom, representative SDS-PAGE of purified protein from top panel plus mononucleosomes used in histone methyltransferase assays. Proteins were visualized by Coomassie staining. The top band contains both EZH2 and SUZ12 (Wang et al., 2017b). Bottom right, histone methyltransferase activity assays using *in vitro* reconstituted mononucleosomes and [^{14}C]S-adenosyl methionine. (B) EZH2 ChIP in cancer cells with relatively high levels of 5mC at the *TERT* promoter. Data are means of three technical replicates + SEM. (C) 5mC levels in relation to ChIP-seq signal H3K27me3 at the *TERT* promoter in HepG2 -124 cells. (D) Kaplan-Meier analysis for 5mC levels at the *TERT* promoter and EZH2 expression for TCGA primary tumors only**.** Stomach cancer shows a converse trend to melanoma, liver cancer and renal papillary cell carcinoma with respect to both 5mC and EZH2 expression. Data from TCGA metastatic tumor samples are omitted in this analysis, reducing the number of patients compared to Figure 5. Top panel, 5mC and bottom panel EZH2 expression levels. Patients were partitioned on methylation levels >0.75, and EZH2 was partitioned on high expression *vs.* low expression, using best separation.

Table S2. Statistical analysis of CCLE lines. Related to Figure 1**.** WT, wild-type at the *TERT* promoter. MUT, -124 or -146 *TERT* promoter mutants, mono_WT, cell lines without known *TERT* promoter mutations exhibiting monoallelic *TERT* expression (Huang *et al.* 2015).

CpG positions	mean_ wt	mean_ mono_	mean_ mut	median_ wt	median_ mono_wt	median_ mut	sdev_w t	sdev_mono _wt	sdev_ mut	std.err _wt	std.err_mono _wt	std.err_ mut	P_wt_vs_ mono	P_wt_vs _mut	P_mut_vs_ mono
1295754:1295760:1295762:1295771:1295772:1295797:1295799	0.902	0.874	0.649	0.956	0.936	0.757	0.160	0.190	0.289	0.011	0.049	0.040	0.299	0.000	0.000
1295681:1295685:1295699:1295705:1295707	0.871	0.836	0.690	0.952	0.931	0.683	0.196	0.188	0.218	0.014	0.050	0.030	0.214	0.000	0.011
1295591:1295594:1295606:1295619	0.813	0.792	0.556	0.926	0.859	0.566	0.253	0.234	0.331	0.018	0.060	0.047	0.445	0.000	0.014
1295431:1295444:1295446:1295454:1295458	0.582	0.496	0.365	0.662	0.559	0.335	0.324	0.323	0.272	0.024	0.083	0.037	0.321	0.000	0.160
1295375:1295377:1295394	0.551	0.450	0.398	0.606	0.355	0.377	0.358	0.345	0.280	0.026	0.086	0.038	0.333	0.005	0.721
1295321:1295338:1295343	0.480	0.410	0.371	0.487	0.444	0.357	0.321	0.283	0.243	0.025	0.073	0.035	0.398	0.044	0.718
1295247:1295257:1295262:1295267:1295274	0.165	0.155	0.097	0.063	0.104	0.055	0.211	0.177	0.135	0.015	0.046	0.020	0.568	0.116	0.739
1295096:1295098:1295100:1295106:1295108:1295117:1295118:1295135:1295139	0.237	0.247	0.302	0.145	0.247	0.248	0.251	0.192	0.253	0.018	0.048	0.034	0.469	0.089	0.635
1294959:1294961:1294963:1294971:1294973:1294974:1294981:1294983:1294995	0.239	0.298	0.363	0.162	0.316	0.362	0.234	0.195	0.273	0.016	0.050	0.037	0.200	0.001	0.454
1294873:1294890	0.175	0.225	0.156	0.060	0.204	0.076	0.227	0.211	0.183	0.016	0.055	0.025	0.243	0.771	0.238